Pathways to Fluorescence via Restriction of Intramolecular Motion in Substituted Tetraphenylethylenes

Journal:	*Physical Chemistry Chemical Physics*
Manuscript ID	CP-ART-10-2021-004848.R1
Article Type:	Paper
Date Submitted by the Author:	05-Dec-2021
Complete List of Authors:	Li, Yingchao; Tianjin University Aquino, Adelia; University of Vienna, Siddique, Farhan ; Bahauddin Zakariya University Niehaus, Thomas; Université Claude Bernard Lyon 1, Lischka, Hans; University of Vienna, Institute for Theoretical Chemistry and Structural Biology Nachtigallova, Dana; Institute of Organic Chemistry and Biochemistry, Molecular Modeling

SCHOLARONE™
Manuscripts

Pathways to Fluorescence via Restriction of Intramolecular Motion in Substituted Tetraphenylethylenes

Yingchao Li,[a] Adélia J. A. Aquino,[a,b] Farhan Siddique,[c,d] Thomas A. Niehaus,[e] Hans Lischka,[a,f]* and Dana Nachtigallová,[g,h]*

[a] School of Pharmaceutical Science and Technology, Tianjin University, Tianjin 300072, PR China

[b] Department of Mechanical Engineering, Texas Tech University, Lubbock, TX, 79409, USA

[c] Department of Pharmaceutical Chemistry, Bahauddin Zakariya University, 60800 Multan, Pakistan

[d] Royal Institute of Medical Sciences, Multan, Pakistan

[e] Univ Lyon, Université Claude Bernard Lyon 1, CNRS, Institut Lumière Matière, F-69622, Villeurbanne, France

[f] Department of Chemistry and Biochemistry, Texas Tech University Lubbock, TX 79409-1061, USA

[g] Institute of Organic Chemistry and Biochemistry v.v.i., The Czech Academy of Sciences, 16610 Prague 6, Czech Republic

[h] IT4Innovations, VŠB-Technical University of Ostrava, 70800 Ostrava-Poruba, Czech Republic

Email: dana.nachtigallova@uochb.cas.cz
Email: hans.lischka@univie.ac.at

Abstract

The design of materials with enhanced luminescence properties is a fast-developing field due to the potential applicability of these materials as light-emitting diodes or for bioimaging. A transparent way to enhance the emission properties of interesting molecular candidates is blocking competing and unproductive non-radiative relaxation pathways by the restriction of intramolecular motions. Rationalized functionalization is an important possibility to achieve such restrictions. Using time-dependent density functional theory (TD-DFT) based on the ωB97XD functional and the semiempirical tight-binding method including long-range corrections (TD-LC-DFTB), this work investigates the effect of functionalization of the paradigmatic tetraphenylethylene on achieving restricted access to conical intersections (RACI). Photodynamical surface hopping simulations have been performed on a larger set of compounds including TPE and ten functionalized TPE compounds. Functionalization has been achieved by means of electron-withdrawing groups, bulky groups which block the relaxation channels via steric hindrance and groups capable of forming strong hydrogen bonds, which restrict the motion via the formation of hydrogen bond channels. Most of the investigated functionalized TPE candidates show ultrafast deactivation to the ground state due to their still existing structural flexibility, but two examples, one containing -CN and -CF$_3$ groups and a second characterized by a network of hydrogen bonds, have been identified as interesting candidates for creating efficient luminescence properties in solution

1   Introduction

Tetraphenylethylene (TPE) received considerable attention in the last decade for its unusual luminescent behavior among carbon-based fluorescent molecules.[1-4] The emission in most conventional organic fluorescents is quenched via aggregation,[5, 6] limiting their use in light-emitting diodes or for bioimaging. Typically, these systems consist of extensive planar aromatic structures in which strong π-π stacking interactions quench the emission upon the aggregation. However, aggregation can also have the opposite effect. For example, after electronic excitation of molecules containing C=C double bonds, radiationless deactivation to the ground state (and therefore quenching of fluorescence) occurs via rotation around these or related bonds. These motions are restricted upon aggregation, thus blocking the non-radiative relaxation channels and leading to enhanced luminescent properties,[7] denominated as aggregation-induced-emission (AIE).[8-10] Among these twisted systems, TPE represents an archetypal luminogen, not emissive in dilute solution but highly emissive in solid-state.[11] Based on these properties, TPE has been used as a major building block to prepare solid state emitters with applications in organic light-emitting diodes[7] and biomolecular science.[12]

The term restriction of intramolecular motion (RIM), which combines intramolecular vibrations and rotations, is generally accepted as the effective molecular mechanism for AIE. However, Tran et al.[13] pointed out that restricted access to the conical intersection (RACI)[14-16] rather than the RIM mechanism as such characterizes the TPE relaxation. Since the discovery of AIE, a great effort has been made to investigate the properties of compounds showing AIE and to develop AIE-based luminescence materials.[6, 17, 18 1, 19 20] As an alternative to aggregation processes to achieve efficient luminescent properties, functionalization by means of molecular substitution has been considered as an interesting alternative since it would provide luminescence as an intrinsic molecular property independent of its aggregation status.

The studies on the excited state dynamics of TPE discuss two main nonradiative deactivation channels, the ethylene twist and the torsional motion of phenyl rings[1-4, 21, 22]. The former movement is further connected with the E/Z (or cis/trans) isomerization;[4] the latter with a cyclization process with a covalent bond formed between the two carbon atoms of two neighboring twisted phenyl rings.[21, 23-25] The photocyclization requires smaller torsional movements of the

phenyl rings and, according to the calculations, proceeds on a shorter timescale than the ethylene twist, which is characterized by more pronounced geometrical rearrangements.[13] However, some controversy appeared in the literature on the assignment of the primary relaxation channel to quench the TPE fluorescence, favoring either ethylene twist[21, 26-30] or the torsional motion of phenyl rings.[31-34] Different levels of calculations have been performed to reveal the main mechanism of TPE excited state relaxation. Applied methods range from time-dependent density functional theory (TD-DFT employing the PBE0 functional) to Time-dependent Density Functional-based Tight Binding (TD-DFTB) calculations,[13, 35] as well as wavefunction-based methods.[23, 36] The results of relaxation dynamics, including the assessment of the dominant relaxation channel, depend on the computational level used to describe the nuclear dynamics and electronic structure of the systems. TD-DFTB is of great interest especially for dynamics simulations because of its enhanced computational efficiency. However, as discussed by Tran *et al.*[13], the results of the (TD-DFTB) calculations differ depending on the description of the long-range corrections. The TD-DFTB description performed without long-range corrections favors the ethylene twist relaxation channel.[35] In contrast, the TD-DFTB with the long-range corrections as implemented by Humeniuk *et al.*[37] (TD-LC1-DFTB) predicted the relaxation solely by photocyclization.[13] On the other side, simulations performed with the LC implementation by Lutsker *et al.*[38] and Kranz *et al.*[39] show the importance of both mechanisms, although photocyclization is preferred.[13] This conclusion matches the results obtained with TD-DFT nonadiabatic dynamics[40], and static second-order complete active space perturbation (CASPT2) calculations, which found a barrierless path towards photocyclization and a barrier of about 8.4 kcal/mol (0.36 eV) for photoisomerization via ethylene twist.

The effects of above-mentioned functionalization of TPE have been debated in terms of strategies for tuning the emission properties, showing quite exciting variability. The goal of the functionalization investigations is to achieve restrictions in the internal molecular motions by inserting different substituents into TPE, which should lead to the RACI effects keeping the molecule in the S_1 state and thus providing sufficient time for fluorescence emission in solution. Gao *et al.*[36] compared the excited-state decay of TPE substituted with four methyl groups in *ortho* or *meta* positions, performing extended static calculations and photodynamics simulations using the semiempirical orthogonalization model 2 (OM2) in combination with multireference configuration interaction (MRCI). In these calculations, the two adjacent phenyl rings are

substituted in the *ortho*-structure, and the two remaining phenyl rings are non-substituted. In contrast, in the *meta*-structure, all phenyl rings are substituted by one methyl group. The results show blocking both relaxation channels by CH_3 substituents in the former structure, while the latter system starts to relax to the ground state at about 200 fs. A combination of steric restriction due to the functionalization and aggregation explains a different emission efficiency of two stilbene-based isomers.[22] Different numbers of methyl groups in *ortho*- positions result in either twisted (one CH_3) or planar (two CH_3) isomers with varying emission properties. The former shows AIE properties, i.e. it is non-emitting as a monomer, while the latter is emissive in both solvent (monomer) and upon aggregation. Interestingly, TPE locked with geminally bridging ethyl groups is silent in emission spectra[21, 41] and brightly fluorescent when geminally locked with an oxygen atom.[42] The computational studies on the optical spectra of these systems, together with geminally substituted methyl- and sulfur-locked TPE, performed by Zhang *et al.*[43] explain the strong emission of oxygen-locked TPE by the effect of both rigidity and an increased conjugation due to oxygen lone pairs.

Introducing heteroatom-containing substituents into TPE brings additional possibilities to modify the luminescent properties, originating from enhanced cooperation via through-space intermolecular interactions upon aggregation.[17] At the same time, heteroatoms contribute to a rather complex character of the excited states, mainly due to their electron-withdrawing or electron-donating characters and/or the existence of lone-pair orbitals involved in excited states.[44, 45] The substituents capable of hydrogen-bond formation represent a particularly interesting class, as they can contribute to the RIM mechanism to slow down the relaxation process.[4] On the other, their excited state dynamics typically occurs on ultrafast time scales[46] and, thus, can significantly modify the lifetimes of TPE-based systems by both inter and intramolecular hydrogen bonds making excited state proton transfer (ESPT) paths available.[47, 48]

Despite a detailed investigation of TPE excited state dynamics, the effect of heteroatom substitutions seems to be promising but has not been explored extensively. This fact has motivated us to study the possibilities of functionalization of TPE more broadly in order to achieve fluorescence emission in solution at molecular basis. Two types of TPE-based systems are considered: (i) substitutions with strongly electron-withdrawing CN and CF_3 groups and (ii) groups capable of forming hydrogen bonds. In total, 11 different substitution types containing -CN, -OH, -CF_3, -CHO, -COOH and -$CONH_2$ groups were selected to explore different possibilities

of restraining the substituted TPE motion including steric hinderances and hydrogen bonds.

Moreover, the dynamics are based on TD-DFT using the long-range corrected ωB97xD[49] functional serving as a reference and using TD-LC-DFTB for comparison and confirmation of DFT results by running for longer simulation times due to the enhanced computational efficiency of DFTB. Verification of the applicability of the LC-DFTB method is of great practical interest with relevance to future applications on related aromatic systems.

2   Computational methods

Optimization of ground-state (S_0) geometries was performed with the ωB97xD functional[49] with the triple-zeta valence polarization (TZVP) basis set[50, 51] and with the long-range corrected DFTB with second-order correction (LC-DFTB2)[38, 39] with the ob2-1-1 Slater-Koster (SK) parameter set.[52] Since fluorine parameters are not available in the ob2-1-1 SK set, for TPE(CN)$_5$CF$_3$, the LC-DFTB2 method is replaced by DFTB2 with the halorg-0-1 SK set.[53-56] In the DFTB calculations, the dispersion interactions were included via a Lennard-Jones potential[57] with parameters adopted from the universal force field (UFF).[58] The electronic excitations were computed using the TD-DFT/ωB97xD and TD-LC-DFTB2 methods. Vertical excitation and emission energies were calculated based on the structures optimized for the S_0 and S_1 states, respectively; the adiabatic energies were computed as the energy difference between the minima of the S_0 and S_1 states.

The initial conditions for the surface hopping dynamics and sampling points for calculating the UV spectra were computed in the framework of the nuclear ensemble approach.[59, 60] Vibrationally broadened UV spectra were generated from 250 sampling points for which ten states were computed for displaced geometries obtained from a harmonic-oscillator Wigner distribution.[61] The same sampling points were used to create the initial conditions of the dynamics within an energy window placed symmetrically around the first absorption peak. For the excited-state dynamics, surface hopping was used in the framework of the fewest switching algorithm[62] corrected for decoherence effects ($\alpha = 0.1$ Hartree).[63] Nonadiabatic interactions were computed following the numerical scheme suggested by Hammes-Schiffer and Tully,[64] and using a local diabatization approximation.[65, 66] 20 trajectories were calculated for each substitution case with a

6

simulation time of up to a maximum of 1 ps for TD-DFT and a maximum of 2 ps for TD-LC-DFTB. In selected cases the simulation time was extended to 5ps for the latter method. The choice of the number of trajectories per case and the simulation times were chosen focusing on the general analysis of a large variety of substitution cases for TPE over the detailed analysis of just a few ones having the substantial computational costs of the simulations in mind. Since the strong mixing between S_0 and S_1 at the crossing between these two states is not represented well by standard DFT methods, we followed previous procedures[67, 68] using a criterion of 0.1 eV for the S_0/S_1 energy gap for stopping the trajectory at that point and taking that time as an estimate for the S_0/S_1 crossing. The dynamics always started from the S_1 state.

The DFTB calculations were performed with a development version of the DFTB+ program.[69] The Gaussian 09 package (Rev.E.01)[70] was used for the ωB97xD calculations. The surface hopping dynamics was carried out with the NEWTON-X program[71] interfaced to DFTB+ and Gaussian 09, respectively.

3   Results and Discussion

3.1   Ground state calculations

Figure 1 and Figure 2 display the TPE structure and the various CN-, OH- and -COOH substituted compounds. The substitutions of the phenyl rings were performed always identically on two phenyl rings. For simplicity, the substitutions are specified for one ring only. Group I contains di-cyano TPE (TPE(CN)), di-penta cyano TPE (TPE(CN)$_5$), di-penta cyano di-hydroxy TPE (TPE(CN)$_5$OH)) and di-penta cyano di-trifluoromethyl TPE (TPE(CN)$_5$(CF)$_3$). Group II includes di-hydroxy di-aldehydo TPE (TPE(OH)(CHO), di-(di-aldehydo) di-(di-hydroxy) TPE (TPE(OH)$_2$(CHO)$_2$), di-hydroxy di-amide TPE (TPE(OH)(CNH$_2$O), di-(di-hydroxy) di-(di-amide) TPE (TPE(OH)$_2$(CNH$_2$O)$_2$), di-hydroxy di-carboxyl TPE (TPE(OH)(COOH)) and di-(di-hydroxy) di-(di-carboxyl) TPE (TPE(OH)$_2$(COOH)$_2$). The listed substituents for group I were chosen to provide electron withdrawing effects and/or steric hindrance through CN and CF$_3$ groups and weak hydrogen bonds with a hydroxy group. Group II contains substituents for establishing strong hydrogen bonds formed between the hydroxy groups, and additional aldehyde, amide, or carboxyl groups. Table 1 and Table 2 display the values of the torsional angles τ(ethyl) around the ethylene double bond and τ(phe) for the phenyl torsion as defined in Figure 1. Note, that in the case of TPE

only one value of τ(phe) is reported due to the C_{4h} symmetry of TPE. The symmetries of other systems lower to C_{2h} and, thus, two values are reported. The ethylene torsional groups show only minor out-of-plane deviations due to the functionalization of the phenyl rings. The torsional angle for TPE is 176° and 174° using the LC-DFTB2 and ωB97XD methods, respectively. This angle changes only a little in CN-functionalized structures, with values between 176° and 180°. The differences between LC-DFTB2 and ωB97XD methods in this torsional angle are not larger than 3°. The OH-functionalization of TPE results in slightly larger out-of-plane deviations, with the largest distortion in TPE(OH)(CHO) and TPE(OH)(COOH) of 172° and 175° obtained at the ωB97XD level, respectively. Although the results of the two methods differ slightly more (up to 7°), their agreement is still reasonably good. The CN-functionalization increases the out-of-plane torsion of the phenyl rings. In TPE(CN)$_5$, the distortion accounts for 16° and 13° at the LC-DFTB2 and ωB97XD, respectively. Additional substitutions with OH and CF_3 groups further modify this value. The OH and COOH functionalization slightly changes the phenyl torsional angles, and the deviations are not larger than 6°. Also in this case, the agreement between the two methods used is reasonably good.
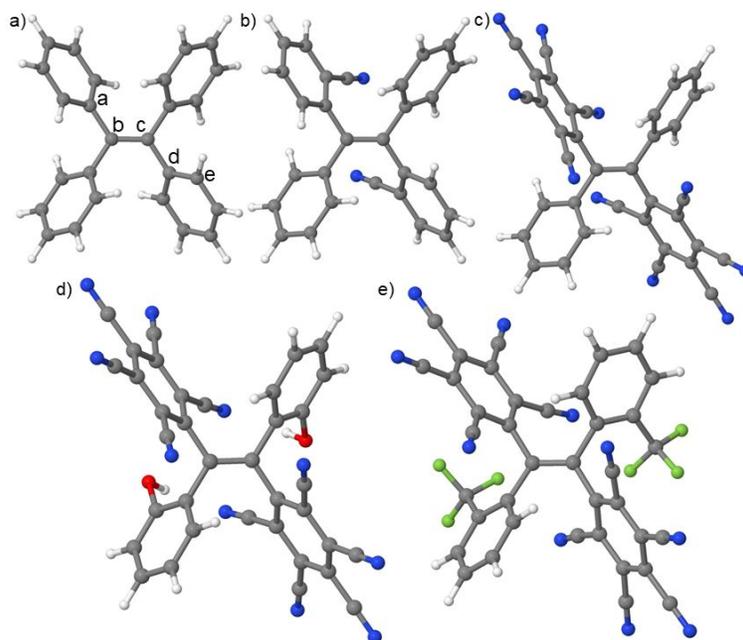
Figure 1. Optimized ground state structures for group I substituted TPE compounds: a) TPE, b) di-cyano TPE, c) di-penta cyano TPE, d) di-penta cyano di-hydroxyl TPE, e) di-penta

cyano di-trifluoromethyl TPE. The torsional angle around the ethylene double bond τ(ethyl) is τ(a,b,c,d) and the phenyl ring torsion τ(phe) is τ(b,c,d,e).
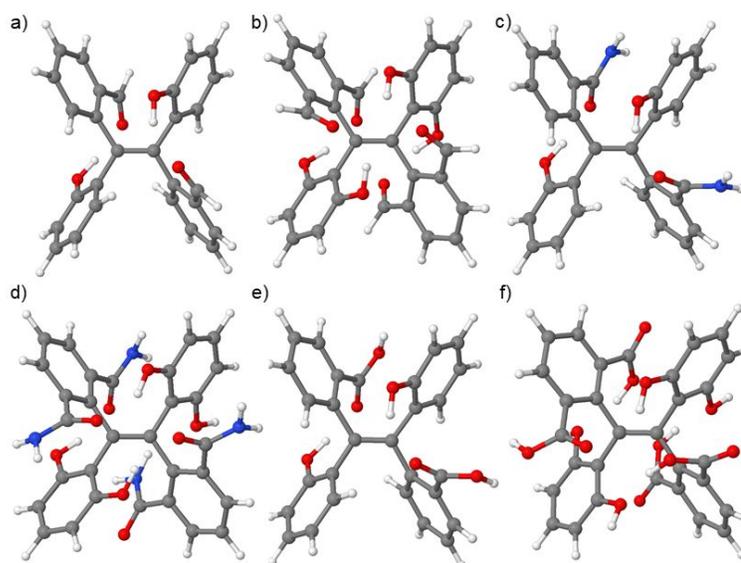
Figure 2. Optimized ground state structures for group II substituted TPE compounds: a) di-hydroxy di-aldehydo TPE, b) di-(di-aldehydo) di-(di-hydroxy) TPE, c) di-hydroxy di-amide TPE, d) di-(di-hydroxy) di-(di-amide) TPE, e) di-hydroxy di-carboxyl TPE, f) di-(di-hydroxy) di-(di-carboxyl) TPE.

Table 1. Ethylene and phenyl torsional angles for TPE and CN-substituted compounds (group I). The angles are defined in Figure 1.

System	Method	Ethylene torsional angle[a]	Torsional angle of phenyl rings[a,b]
TPE	LC-DFTB2	--[c]	--[c]
		176.1	*53.6*
	ωB97XD	102.7	19.8
		174.4	*52.7*
TPE(CN)	LC-DFTB2	114.2	19.3; 19.6(CN)
		178.1	*50.7; 64.2(CN)*
	ωB97XD	123.9	24.0; 26.8(CN)
		176.1	*51.7; 60.2(CN)*
TPE(CN)$_5$	LC-DFTB2	126.4	26.1; 30.8 (CN)
		179.8	*55.5; 70.2(CN)*
	ωB97XD	137.4	30.6; 36.7(CN)
		176.3	*52.8; 67.2(CN)*
TPE(CN)$_5$OH	LC-DFTB2	--[c]	--[c]
		175.6	*60.2(OH); 73.9(CN)*

			HB^d: 2.59 *2.50*
	ωB97XD	140.5	35.3(OH); 37.0(CN)
		178.4	*59.1(OH); 67.8(CN)*
			HB^d: 1.93 *2.14*
TPE(CN)$_5$CF$_3$	DFTB2-halorg-0-1	165.2	39.3 (CF$_3$); 44.9 (CN)
		178.9	*49.4(CF$_3$); 62.8(CN)*
	ωB97XD	165.5	38.6 (CF$_3$); 44.1 (CN)
		178.4	*40.4 (CF$_3$); 62.8 (CN)*

^{a}ground-state optimized values are shown in italics, ^{b}averaged value, ^{c}geometry optimization not converged for the S$_1$ state. ^{d}Hydrogen Bond distance (in Å)

Table 2. Ethylene and phenyl torsional angles and hydrogen bonds for TPE substituted by OH-, and CHO-, COOH- and CONH$_2$- groups (group II). The angles are defined in Figure 1.

System	Method	Ethylene torsional angle^a	Torsional angle of phenyl rings^a
TPE(OH)(CHO)	LC-DFTB2	172.2	OH: 53.0, 71.4 CHO: 65.6, 74.3
		179.9	*OH:76.6, 115.3, CHO: 80.8, 103.3*
		HB^b: 1.78 – 1.99 (2); *1.86 – 1.87 (2)*	
	ωB97XD	163.4	OH: 48.0, 65.5 CHO: 43.5, 65.6
		172.5	*OH: 62.2, 75.1 CHO: 64.9, 75.0*
		HB: 1.77 – 1.98 (2); *1.90 – 1.98 (2)*	
TPE(OH)(COOH)	LC-DFTB2	--^{c}	--^{c}
		176.8	*OH: 62.3, 79.3 COOH: 63.3, 80.2*
		HB: *1.833 – 1.865 (2)*	
	ωB97XD	159.6	OH: 41.7, 61.2 COOH: 31.8, 53.8
		175.0	*OH: 60.2, 69.0 COOH: 62.8, 67.6*
		HB: 1.931 – 2.300 (2); *1.876 – 2.002 (2)*	
TPE(OH)$_2$(CHO)$_2$	LC-DFTB2	163.4	OH^d: 46.7, CHO^d: 58.2
		176.6	*OH^d: 57.8, CH^d: 62.7*
		HB: 1.915 – 2.484 (6); *1.898 – 2.254 (3)*	
	ωB97XD	179.8	OH^d: 55.4, CHO^d: 50.5
		176.2	*OH^d: 57.3, CHO^d: 59.2*
		HB: 1.711 – 2.376 (6); *1.994 – 2.217 (3)*	
TPE(OH)$_2$(COOH)$_2$	LC-DFTB2	171.3	OH: 43.5, 56.3, COOH: 25.6, 53.3
		179.4	*OH: 48.7, 56.1 COOH: 54.1, 60.9*
		HB: 1.914 – 2.064 (3); *1.889 – 2.029 (3)*	
	ωB97XD	175.3	OH: 47.7, 53.6; COOH: 39.4, 49.2
		176.7	*OH: 49.4, 57.9 COOH: 54.0, 61.2*
		HB: 1.820 – 2.413 (7); *1.927 – 2.522 (4)*	
TPE(OH)(CONH$_2$)	LC-DFTB2	170.9	OH: 48.7, 71.9; CONH$_2$: 53.9, 72.2
		178.3	*OH: 61.1, 73.7 CONH$_2$: 61.3, 74.8*
		HB: 1.839 – 1.969 (2); *1.844 – 1.886 (2)*	
	ωB97XD	160.9	OH: 38.8, 62.5; CONH$_2$: 31.0, 55.5
		177.1	*OH: 60.7, 69.0 CONH$_2$: 63.3, 67.7*

			HB: 1.901 – 2.206 (2); *1.850 – 1.969 (2)*
TPE(OH)$_2$(CONH$_2$)$_2$	LC-DFTB2	177.1	OH: 49.7, 52.6; CONH$_2$: 44.8, 59.5
		176.5	*OH: 52.7, 57.6 CONH$_2$: 51.4, 61.6*
			HB: 1.828 – 2.071 (3); *1.908 – 2.349 (5);*
	ωB97XD	175.6	OH: 45.3, 53.7; CONH$_2$: 43.1, 46.5
		177.7	*OH: 53.8, 57.2 CONH$_2$: 61.4, 52.5*
			HB: 1.858 – 2.422 (6); *1.937 – 2.366 (4)*

[a]the ground-state optimized values are shown in italics, [b]Hydrogen Bond distance (in Å), the number in parentheses indicates the number of HBs (< 2.5 Å); [c]geometry optimization not converged for the S$_1$ state., [d]averaged value

3.2   Absorption spectrum

Vertical absorption energies of TPE and CN-substituted compounds, oscillator strengths and orbital transitions are given in Table 3 and Table 4 for the first excited state of each compound using the TD-DFT/ωB97XD and TD-LC-DFTB2 methods. Tables S1-S11 contain results for the first ten states. HOMO/LUMO orbital pairs are depicted in Figure S1. The calculations using the ωB97XD functional give the first excited state of TPE at 4.342 eV (Table 3). The sizable spatial overlap between the HOMO and LUMO orbitals (Figure S1a), mainly involved in the electronic transition of the first excited state, explains its bright character. The second and third excited states are separated by energy gaps of 0.6 and 0.7 eV (Table S1), respectively, with significantly smaller oscillator strengths. These results closely match with the previously reported excitation energies and oscillator strengths[13] obtained with DFT employing long-range corrected CAM-B3LYP and LC-ωPBE functionals and with the second-order algebraic diagrammatic construction (ADC(2)) method, and with experimental observations which find the first absorption bands measured in tetrahydrofurane at ~4 eV.[72] Functionalization of TPE by one CN group changes this picture somewhat; a small spatial overlap between HOMO and LUMO components of the phenyl rings (Figure S1b) decreases the oscillator strength of the first excited state (Table 3). Additionally, the nature of the second and third excited states (Table S2) are separated by a smaller energy gap from the first excited state as compared to TPE. These states are almost degenerate at both computational levels. The sizable overlap between the HOMO and LUMO+1 in the S$_2$ transition, observed with ωB97XD, explains the oscillator strength value comparable to that of the 1st excited state. Thus, also, the higher excited states (2nd and 3rd with the ωB97XD and LC-DFTB2, respectively) will contribute to the absorption spectra of TPE(CN). The good agreement between the ωB97XD and

LC-DFTB2 results justifies the use of the latter method for further dynamics simulations.

Table 3. Vertical excitations listed for the first excited state for group I compounds using the TD-LC-DFTB2/ DFTB2-halorg-0-1 and ωB97xD approaches. The transition is always from HOMO to LUMO.

Method	State	Excitation energies (eV)	Oscillator strength
TPE			
TD-LC-DFTB2	1	4.673	0.558
ωB97xD	1	4.342	0.424
TPE(CN)			
TD-LC-DFTB2	1	4.687	0.324
ωB97xD	1	4.324	0.256
TPE(CN)$_5$			
TD-LC-DFTB2	1	4.157	0.016
ωB97xD	1	3.694	0.016
TPE(CN)$_5$(OH)			
TD-LC-DFTB2	1	3.653	0.005
ωB97xD	1	3.776	0.014
TPE(CN)$_5$(CF$_3$)			
DFTB2-halorg-0-1	1	3.009	0.186
ωB97xD	1	3.846	0.302

Table 4. Vertical excitations listed for the first excited state for group II compounds using the TD-LC-DFTB2 and ωB97xD approaches.

Method	State	Excitation energies(eV)	Oscillator strength	Transition[a]
TPE(OH)(CHO)				
TD-LC-DFTB2	1	3.671	0.000	H-2 → L
ωB97xD	1	3.724	0.040	H → L
TPE(OH)(COOH)				
TD-LC-DFTB2	1	4.343	0.021	H-2 → L
ωB97xD	1	4.189	0.144	H → L
TPE(OH)(CONH$_2$)				
TD-LC-DFTB2	1	4.475	0.033	H-1 → L
ωB97xD	1	4.329	0.180	H → L
TPE(OH)$_2$(CHO)$_2$				
TD-LC-DFTB2	1	3.979	0.057	H-2 → L
ωB97xD	1	3.616	0.059	H-2 → L
TPE(OH)$_2$(COOH)$_2$				

TD-LC-DFTB2	1	4.154	0.151	H $\rightarrow$ L
ωB97xD	1	4.080	0.125	H-1 $\rightarrow$ L
TPE(OH)$_2$(CONH$_2$)$_2$				
TD-LC-DFTB2	1	4.150	0.104	H $\rightarrow$ L
ωB97xD	1	3.975	0.130	H-1 $\rightarrow$ L

^{a} H stands for HOMO and L for LUMO

The character of the spectrum changes dramatically with an increased number of CN groups in TPE(CN)$_5$. The electron-withdrawing CN groups cause significant changes in the nature of the LUMO (Figure S1c), in which the electron density concentrates on the CN-substituted phenyl rings. As a result, there is a vanishing spatial overlap between HOMO and LUMO, leading to a negligible oscillator strength for the first excited state. The electron-withdrawing CN groups stabilize the LUMO and consequently shift the absorption spectrum's origin to lower energies. The higher excited states, resulting from the HOMO $\rightarrow$ LUMO+1 (second excited state) and LUMO+2 (third excited state), are even more affected, being now in the same energy range as the first excited state and more intense. Although all excitation energies shift to larger values with LC-DFTB2, this method gives similar absorption spectra characters in both systems.

The ωB97XD calculations do not predict dramatic changes in the spectra with additional OH- functionalization (Table S4), resulting in the same spectra characters as TPE(CN)$_5$. On the contrary, the changes in the LUMO character of TPE(CN)$_5$(CF$_3$), in particular a sizeable contribution from the central carbon atoms, (Figure S1e), increase the orbital overlap between HOMO and LUMO and thus the oscillator strength value of the first excited state (Table S5). Comparing the character of the spectra across the investigated TPE(CN)$_5$ systems shows a prevailing effect of the CN- over the OH- and CF$_3$- groups.

It is important to note that LC-DFTB2 calculations provide the same characteristics in terms of energy gaps of individual states and oscillator strengths introduced by OH and CF$_3$ functionalization; the excitation energies of the latter system are, however, underestimated by ~0.8 eV with respect to those obtained with the ωB97XD functional. This unusual large deviation of the DFTB results in this case is certainly related to the absence of the long-range correction and the use of a different parametrization for fluorine.

Table 4 and Tables S6 to S11 compare the results of the LC-DFTB2 and ωB97XD calculations of the absorption spectra of group II TPE functionalized compounds containing OH

group and additional CHO, COOH, and $CONH_2$ groups. As in the previous cases, the functionalization lowers the excitation energies and the oscillator strengths. Contrary to CN-functionalized TPEs, the discussed excited states result in several instances from energetically lower occupied orbitals, e.g., HOMO-1 and HOMO-2. Still, the electronic transitions in these states appear solely within the π-system.

Comparison of LC-DFTB2 and ωB97XD shows again a reasonably good agreement. In most cases, the differences in the excitation energies are within 0.2 eV, and the largest differences do not exceed 0.4 eV. Also, the character of spectra in terms of oscillator strengths are described similarly.

3.3 S_1 state properties

The fluorescence spectra of TPE and functionalized TPE systems are evaluated based on the vertical emission energies starting from the optimized geometries of the S_1 state. The geometry changes in the S_1 excited states are primarily discussed based on the results obtained with ωB97XD optimization. The LC-DFTB2 method gives very similar results.

Table 1 and Table 2 compare the torsional angles obtained from S_1 excited-state optimization for TPE and group I, and group II substitutions, respectively, with the respective ground state values. The corresponding adiabatic energies and the vertical emission energies are displayed in Table 5 and Table 6, respectively. The torsion around the central ethylene double bond of all TPE and CN-functionalized TPE systems deviates significantly from the ground-state planarity upon excitation. The distortion is most pronounced in non-functionalized TPE, resulting in the dihedral angle of ~103° for the S_1 state at the ωB97XD level in comparison to 174° for the ground state. The CN-functionalization reduces the distortion somewhat, leading to the dihedral angles of ~123° and ~137° for TPE(CN) and TPE(CN)$_5$, respectively. Additional substitutions with OH and CF_3 groups further restrict the distortion; the ωB97XD optimization gives values of only 141° and 165° for TPE(CN)$_5$(OH) and TPE(CN)$_5$(CF$_3$), respectively. The TD-LC-DFTB2 calculations lead in these cases to smaller torsional angles for the S_1 state where available (TPE(CN): 114°, TPE(CN)$_5$: 126°).

The phenyl rings of TPE, which are significantly rotated with respect to the ethylene π-bond in the ground state (dihedral angle of ~53°), are planarized in the S_1 minimum to ~20°. The situation is similar for free phenyl rings of TPE(CN) and TPE(CN)$_5$ (Table 1). The planarization

14

is also observed in functionalized phenyl rings, although to a smaller extent. However, due to the larger distortion of these rings in the ground state, the resulting reduction of the dihedral angle in the S_1 minima is still more significant than that of non-functionalized phenyls. Additional functionalization with OH and CF_3 groups provides similar pictures. The TD-LC-DFTB2 method leads to similar results concerning the changes from S_0 to S_1 in the torsional angles of the phenyl rings.

The ωB97XD adiabatic S_0/S_1 energy differences for TPE and the group I compounds (Table 5) show a relatively narrow energy range (0.6 – 1.2 eV) of S_1 minima stabilization energies across the systems, while there is an even larger red-shift in vertical emission spectra within the range of 1.2 - 2.6 eV. The increasing emission energy in the order TPE < TPE(CN) < TPE(CN)$_5$ < TPE(CN)$_5$(OH) < TPE(CN)$_5$(CF$_3$) correlates reasonably well with the changes of the ethylene torsional angle, with the largest difference for TPE (70°) and the smallest for TPE(CN)$_5$(CF$_3$) (15°). LC-DFTB2 results show the same trends; however, the emission energies tend to be underestimated compared to ωB97XD values by 0.4-0.6 eV.

The torsional angle around the central ethylene π-bond of group II OH-, and CHO-, COOH- and CONH$_2$-functionalized TPE changes from ~180° in the ground state by only ~10° in the S_1 excited state of singly functionalized TPE's (TPE(OH)(CHO), TPE(OH)(COOH), TPE(OH)(NH$_2$)). The angle remains almost unchanged in doubly functionalized TPE's (TPE(OH)$_2$(CHO)$_2$, TPE(OH)$_2$(COOH)$_2$, TPE(OH)$_2$(NH$_2$)$_2$). Similarly, the changes in the dihedral angles of the phenyls rings are smaller in all systems, not larger than 20° (cf. the changes of ~ 33° for non-functionalized phenyls). The smaller flexibility results from both the bulky character of the functional groups and hydrogen bonds formed in these systems. Analysis of the singly functionalized systems shows the existence of two hydrogen bonds (taking a threshold value of 2.5 Å for the X-H⋯A proton donor/acceptor bond as the definition of a hydrogen bond, Table 2) in both S_0 and S_1 minima, with slightly increased distances in the latter structures. The number of hydrogen bonds increases in all doubly functionalized TPE systems upon excitation. This indicates a strengthening of the hydrogen-bonded chain in the excited states, which, in turn, affects the excited state relaxation dynamics (see below).

In line with significantly smaller changes of geometry parameters in the S_1 states, the stabilization energies in S_1 states and the red-shifts of the emission spectra for the group II compounds calculated with ωB97XD are smaller than CN-functionalized (group I) TPE systems.

15

Group II stabilization energies, taken as a difference between vertical and adiabatic excitation energies, are in the range of 0.5 – 0.8 eV (see Table 6) as compared to above-mentioned stabilization energies of 0.6 – 1.2 eV for group I compounds. Similar results are obtained with LC-DFTB2, again with an underestimation of the emission by 0.2-0.6 eV.

Tables 5 and 6 also show the values of the oscillator strengths calculated for vertical emission from the S_1 minimum. Contrary to the absorption spectra, in which the oscillator strengths significantly diminish upon functionalization (Tables S1-S11), for emission, these values are even somewhat larger for group I as compared to the oscillator strength of TPE compounds and are only slightly smaller (with some exceptions) for group II compounds. It should be noted that the intensity of the fluorescence emission is actually proportional to $\sim (\Delta E)^2 f$.[73] The additional dependence on the excitation energies does not influence the conclusion that the fluorescence intensity of the substituted TPE compounds should be comparable to the one of TPE.

Table 5. Adiabatic S_0/S_1 energy differences, vertical emission energies and oscillator strengths for TPE and CN-substituted compounds.

System	Method	Adiabatic energy (eV)[a]	Emission energy (eV)	Oscillator strength
TPE	LC-DFTB2	--[b]	--[b]	--[b]
		4.67		
	ωB97XD	3.30	1.24	0.106
		4.34		
TPE(CN)	LC-DFTB2	3.00	1.15	0.079
		4.69		
	ωB97XD	3.00	1.72	0.131
		4.23		
TPE(CN)$_5$	LC-DFTB2	3.05	1.62	0.220
		4.16		
	ωB97XD	2.81	2.00	0.214
		3.69		
TPE(CN)$_5$OH	LC-DFTB2	--[b]	--[b]	--[b]
		3.65		
	ωB97XD	2.70	1.75	0.144
		3.78		
TPE(CN)$_5$CF$_3$	DFTB2-halorg-0-1	2.70	2.35	0.261
		3.01		
	ωB97XD	3.23	2.60	0.252

<div align="center">

3.85

</div>

[a]Vertical absorption energies of S_1 states are given in italics, [b]geometry optimization not converged for the S_1 state.

Table 6. Adiabatic S_0/S_1 energy differences, vertical emission energies and oscillator strengths for TPE substituted by OH-, and CHO-, COOH- and $CONH_2$- groups.

System	Method	Adiabatic energy (eV)[a]	Emission energy (eV)	Oscillator strength
TPE(OH)(CHO)	LC-DFTB2	3.07	2.16	0.008
		3.67		
	ωB97XD	3.03	2.31	0.029
		3.72		
TPE(OH)(COOH)	LC-DFTB2	--[b]	--[b]	--[b]
		4.34		
	ωB97XD	3.41	2.55	0.077
		4.19		
TPE(OH)$_2$(CHO)$_2$	LC-DFTB2	2.69	1.79	0.010
		3.98		
	ωB97XD	3.01	2.36	0.030
		3.62		
TPE(OH)$_2$(COOH)$_2$	LC-DFTB2	3.53	2.59	0.096
		4.15		
	ωB97XD	3.47	2.82	0.074
		4.08		
TPE(OH)(CONH$_2$)	LC-DFTB2	3.50	2.47	0.027
		4.48		
	ωB97XD	3.55	2.65	0.095
		4.33		
TPE(OH)$_2$(CONH$_2$)$_2$	LC-DFTB2	3.41	2.45	0.021
		4.15		
	ωB97XD	3.46	2.90	0.123
		3.98		

[a]Vertical absorption energies of S_1 states are given in italics, [b]geometry optimization not converged for the S_1 state.

3.4   Photodynamics simulations.

The selection of the initial conditions for each system, particularly the initial excitation energy, has been made based on their simulated absorption spectra (see Figure 3 and Figure 4 for

calculated spectra and the energy window used for the initial conditions in dynamics simulations). All spectra reveal a significant vibrationally broadening shape. The shapes of the absorption spectra simulated with the LC-DFTB2 (Figures S2 and S3) and ωB97XD (Figure 3 and Figure 4) methods are very similar. Due to the large energy gap between the first and higher excited states in TPE (Figure 3 and Figure S2, Table S1), the initial energy spans only the former. In the other systems in which this gap reduces, the initial energy overlaps with higher excited states (Figure 3 and Figure S2 for group I, Figure 4 and Figure S3 for group II, and Tables S2-S11). With Kasha's rule in mind, one can expect the critical relaxation events happening between the ground state and the first excited states. Thus, and also for computational efficiency, the dynamics simulations start from the S_1 state in each case.
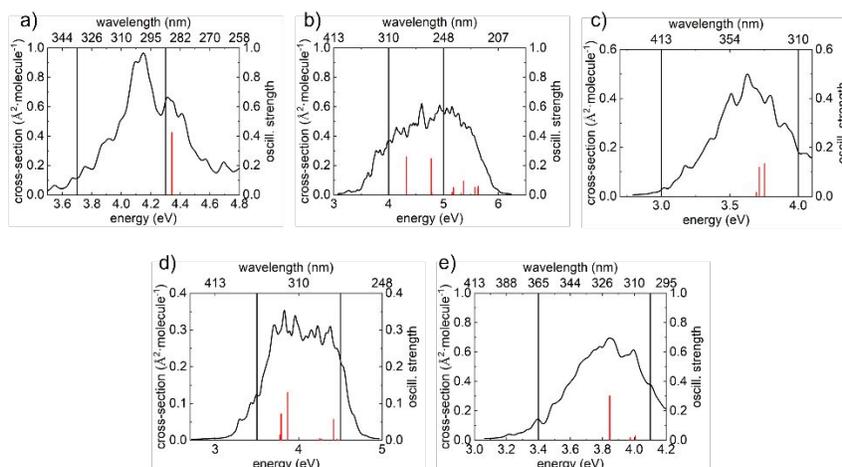
Figure 3. Simulated spectra for group I substituted TPE compounds: a) TPE, b) TPE(CN)$_2$, c) TPE(CN)$_5$, d) TPE(CN)$_5$OH, e) TPE(CN)$_5$CF$_3$. Vertical black lines indicate the boundaries of the window for the initial conditions of the dynamics; vertical red lines specify the calculated vertical excitation energies.
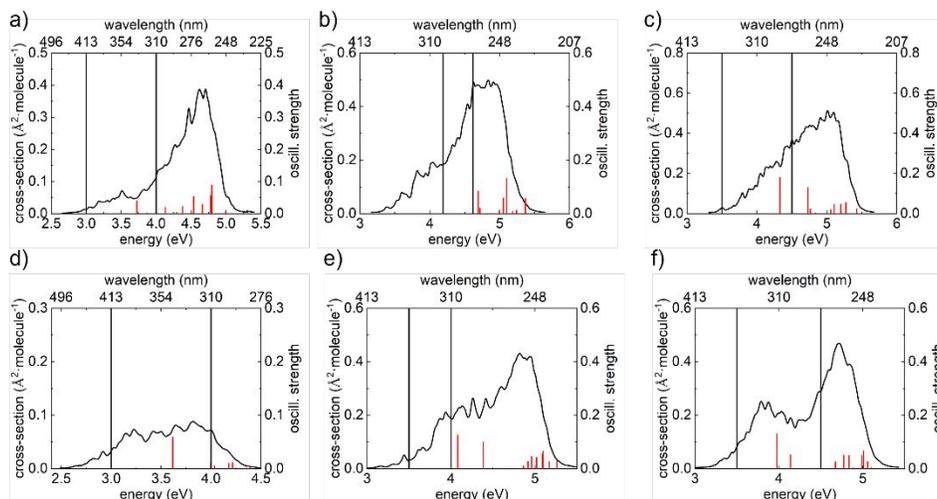
Figure 4. Simulated spectra for group II substituted TPE compounds: a) TPE(OH)(CHO), b) TPE(OH)(COOH), c) TPE(OH)(CONH$_2$), d) TPE(OH)$_2$(CHO)$_2$, e) TPE(OH)$_2$(COOH)$_2$, f) TPE(OH)$_2$(CONH$_2$)$_2$. Vertical black lines indicate the boundaries of the window for the initial conditions of the dynamics; vertical red lines specify the calculated vertical excitation energies.

Both ωB97XD and LC-DFTB2 dynamics simulations show a fast S$_1$ → S$_0$ decay of TPE and TPE(CN) within about 500 fs (Table 7, Figure S15a,b, S16a,b). 20% of the trajectories of the TPE dynamics relaxed within less than 200 fs in the dynamics simulations with LC-DFTB2. The photodynamics and the relaxation process are analyzed by monitoring the energy gap between the ground and first excited states (ΔE(S$_1$/S$_0$)), the ethylene torsional angle τ$_{ethyl}$, and the torsional angle τ$_{phe}$ of the phenyl rings. In the case of longer-lived trajectories (~500 fs), the relaxation proceeds (Figure 5, S7-S10) via a simultaneous motion characterized by a monotonic increase of the ethylene torsional angle from planarity to ~80° and a faster movement of the phenyl rings during which the torsional angles first decrease from ~50° to ~20° at about 200 fs and then turn back to higher values at about 300 fs before they reach values of ~0°. The above-mentioned short-lived trajectories relaxing within 200 fs correspond to photocyclization. Functionalization in TPE(CN)$_5$ slows down the relaxation motion (see Figure 6, S12 and Figure 7, S11, S29c for ωB97XD and LC-DFTB2 simulations). It takes about 750 fs to reach the plateau at ~140° for the torsional angle of CN-substituted phenyl rings (Figure 6d and Figure 7d). The motion of unsubstituted phenyl rings is much faster, with the dihedral angle oscillating initially between ~50°

19

to 0° (Figure 6c and Figure 7c). In the LC-DFTB2 simulations, this value stabilizes at ~ 1.5 ps and the system hops to the ground state. The changes in $\Delta E(S_1-S_0)$ follow similar patterns for the ωB97XD and LC-DFTB dynamics. In the former case, the energy difference decreases quite monotonically and reaches a value of somewhat less than 2 eV at the end of the simulation time. In the latter case, a similar, even stronger, decrease can be seen until 1 ps. Then the energy difference fluctuates around 1 eV until it drops to the ground state at the average hopping time of 1.550 ps (Figure 7). Based on the similarity of the time evolution of $\Delta E(S_1-S_0)$ observed for LC-DFTB2 and ωB97XD within 1 ps, we expect that the lack of deactivation to the ground state obtained with the ωB97XD dynamics simulation results from the too short simulation time (1 ps) rather than from differences in the electronic structure description between the two methods. Thus, also the ωB97XD dynamics is expected to lead to radiationless deactivation to the ground state. Comparison of the TPE, TPE(CN), and TPE(CN)$_5$ relaxation courses indicates that the motion of CN-substituted phenyl rings rule the overall relaxation process.
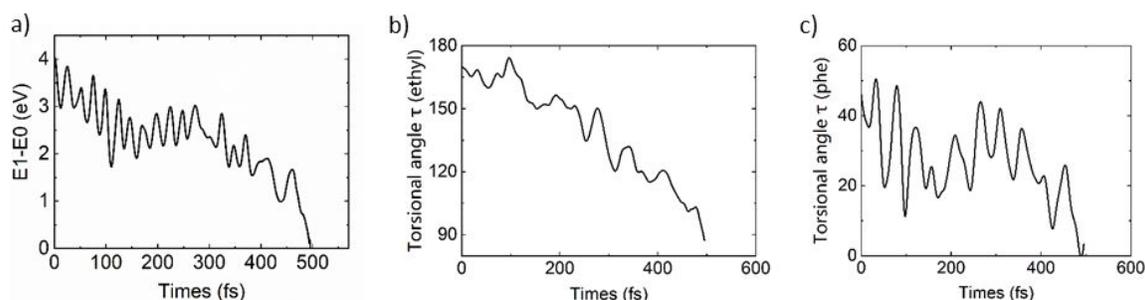
Figure 5. Time evolution of the energy gap $\Delta E(S_1/S_0)$ and the torsional angles τ(ethyl) and τ(phe) for TPE using ωB97XD dynamics simulations of one typical trajectory.

20
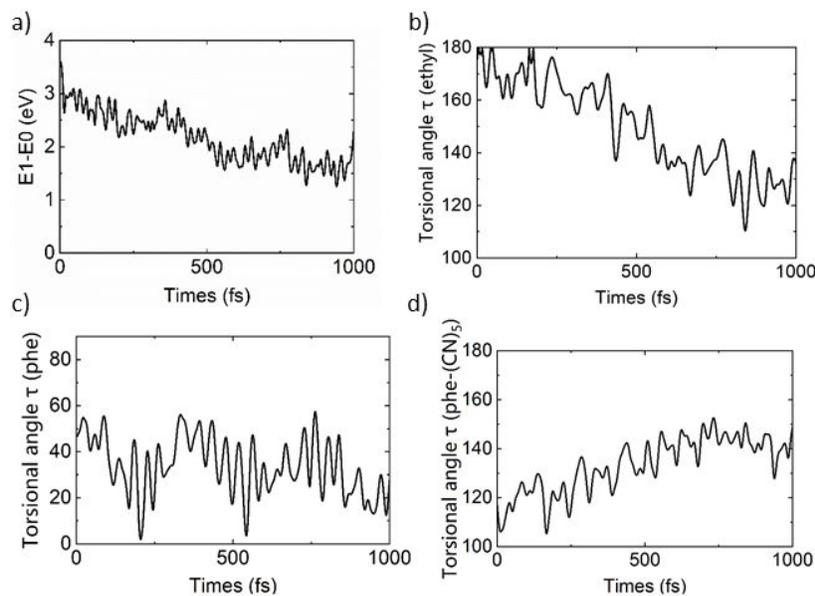
Figure 6. Time evolution of the energy gap $\Delta E(S_1/S_0)$ and the torsional angles τ(ethyl) and τ(phe) for TPE(CN)$_5$ using ωB97XD dynamics simulations.
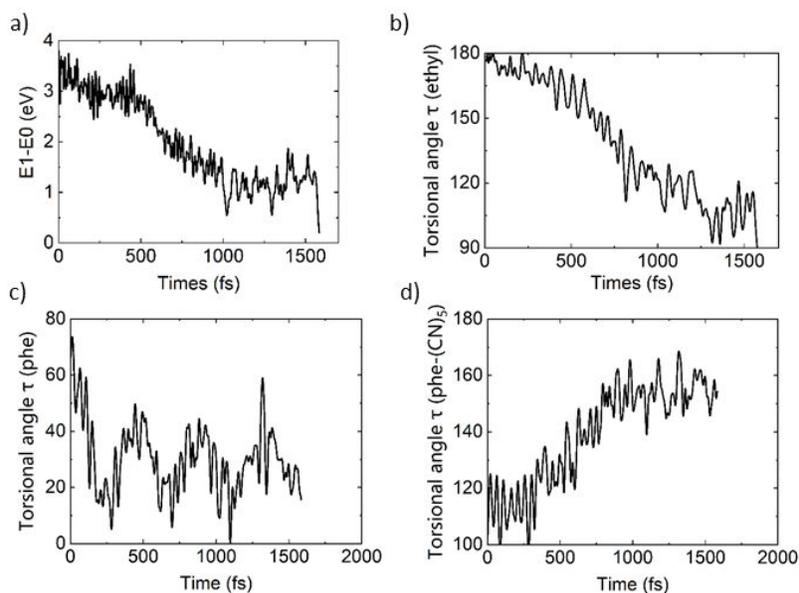
Figure 7. Time evolution of the energy gap $\Delta E(S_1/S_0)$ and the torsional angles τ(ethyl) and τ(phe) for TPE(CN)$_5$ using LC-DFTB2 dynamics simulations.

Table 7. Fraction of trajectories in S_1, characterization of structures at hopping time and average hopping times t_{hop} for TPE, and functionalized TPE compounds derived from surface hopping dynamics performed at the ωB97XD and LC-DFTB2 levels, respectively.

	S_1 state[b]	CCdist/Planar[c]		Planar[d]		ESPT[e]		Pyram[f]	
	%	%	t_{hop}	%	t_{hop}	%	t_{hop}	%	t_{hop}
ωB97XD[a]									
TPE	0	100	516	--		--		--	
TPE(CN)	0	100	570	--		--		--	
TPE(CN)$_5$	[100][g]								
TPE(CN)$_5$(OH)	40		--		--	60	140	--	
TPE(CN)$_5$(CF$_3$)	100		--		--		--		--
LC-DFTB2[a]									
TPE	0	80	507	20	157	--		--	
TPE(CN)	0	100	501	--		--		--	
TPE(CN)$_5$	5	95	1519	--		--		--	
TPE(CN)$_5$(OH)[h]	90	5	5000	--		--		--	
TPE(CN)$_5$(CF$_3$)	100		--		--		--		--
ωB97XD[a]									
TPE(OH)(CHO)	0		--	5	802	95	117	--	
TPE(OH)(COOH)	0		--		--	100	146	--	
TPE(OH)(CONH$_2$)	15		--		--	85	326	--	
TPE(OH)$_2$(CHO)$_2$	0		--		--	100	159	--	
TPE(OH)$_2$(COOH)$_2$	85		--		--	15	374	--	
TPE(OH)$_2$(CONH$_2$)$_2$	40		--		--	60	518	--	
LC-DFTB2[a]									
TPE(OH)(CHO)	25	5	1684	25	781	20	278	25	321
TPE(OH)(COOH)	10		--	30	136	50	131	5	396
TPE(OH)(CONH$_2$)	20		--	60	247	25	212	--	
TPE(OH)$_2$(CHO)$_2$	50		--		--	45	274	5	1589
TPE(OH)$_2$(COOH)$_2$	70		--		--	30	413	--	
TPE(OH)$_2$(CONH$_2$)$_2$	10		--	10	1058	80	630	--	

[a]The simulation time: 1ps (ωB97XD) and 2 ps (LC-DFTB) unless indicated otherwise; [b]the fraction of trajectories which remains in the S_1 state during the whole simulation; [c-f]the fraction of trajectories and the average hopping time (in fs) that relax via a combined ethylene bond distortion/phenyl ring planarization (c); phenyl ring planarization (d); excited-state proton transfer (e); pyramidalization of the central CC double bond (f); [g]estimated strong reduction for longer simulation time (see text for explanation) [h]the simulation time 5 ps.

The additional functionalization leading to TPE(CN)$_5$(CF$_3$) and TPE(CN)$_5$(OH) show strikingly different pictures. The former's relaxation dynamics shows no tendency for $S_1 \rightarrow S_0$ relaxation. Indeed, all trajectories remain in the S_1 state for the whole simulation time, i.e., 1 ps (ωB97XD) (Figure S5a, S13) and 2 ps (LC-DFTB2) (Figure S6a, S14). Minimal fluctuations of torsional angles of the substituted phenyl rings (Figures S5c,d and Figures S6c,d) in comparison

to the respective angles in TPE(CN$_5$) demonstrate the steric hindrance due to the CF$_3$ group. Moreover, the fact that functionalization with one CN group does not change the dynamics course of TPE via complete radiationless deactivation and functionalization with five CN groups only slows down the nonradiative relaxation implies that the electron-withdrawing effect does not play any significant role in the relaxation dynamics. Our results show significant differences between the results of the two computational methods for TPE(CN)$_5$(OH) (Table 7, Figures S15d and S16c). While the ωB97XD simulations predict ultrafast relaxation dynamics, with the averaged hopping time of 140 fs for 60% of trajectories and 40 % of trajectories surviving 1 ps, all trajectories stay in the S$_1$ state in the LC-DFTB2 simulations, except two which relax at ~4.5 ps. The time evolutions of the ethylene and CN-phenyl torsional angles are similar; the motion of OH-phenyl rings is suppressed and slower than unsubstituted phenyls in TPE(CN)$_5$ due to hydrogen bonds formed between OH and CN groups of neighboring phenyls (Figures S17, S18). While these hydrogen bonds remain bonded in all trajectories of the LC-DFTB2 dynamics simulations, the relaxation in the short-lived trajectories in ωB97XD simulations is accompanied by OH → CN ESPT (Figure 7).

The effect of OH-functionalization is further demonstrated by the relaxation of the OH-functionalized systems (Figure S20). Except for TPE (OH)$_2$(COOH)$_2$ (see below), the majority of trajectories relax to the ground state within ~ 200 fs for most systems. The short-time course of these dynamics does not allow for significant changes in ethylene and phenyl torsional angles. The ESPT is the driving force for the S$_1$ → S$_0$ decay in the vast majority of TPE(OH)(CHO) and TPE(OH)$_2$(CHO)$_2$ and TPE(OH)(COOH) ultrafast relaxation, on the timescale less than 200 fs, obtained with the ωB97XD simulation Figure S20a,b,e). Similar fast intermolecular ESPT processes have also been observed in the S$_1$ dynamics of 3-hydroxyflavone connected to water clusters.[48] The OH → CHO transfer realizes the ESPT. Additionally, photocyclization leading to furan formation via (CHO) has been observed as an additional possible relaxation channel. However, this channel has been observed for only one trajectory (Table 7), TPE(OH)(CHO) in the ωB97XD dynamics.

LC-DFTB2 dynamics simulations provide a somewhat modified picture (Figure S19). Despite the fast nonadiabatic deactivation to the ground state, realized via ESPT and photocyclization, accounting for 20% of trajectories together, for TPE(OH)(CHO) about the same number of trajectories (30%) deactivate via the pyramidalization of the ethylene subunit. This

happens also to a lesser extent for TPE(OH)(COOH) and TPE(OH)$_2$(CHO)$_2$. Notably, there are still trajectories that remain in the S$_1$ state during the simulation time of LC-DFTB2 dynamics. As in the wB97XD dynamics simulations, the ethylene torsional angle changes do not show any tendency for the comparable C-C distortion observed in TPE and the group I compounds. An increasing number of hydrogen bonds in the systems correlates with a more significant fraction of trajectories that survive in the excited state during the LC-DFTB2 simulations, particularly 25% and 50% in TPE(OH)(CHO) and TPE(OH)$_2$(CHO)$_2$. A network of co-existing hydrogen bonds makes the system less flexible, as it is apparent from the time evolutions of all monitored angles of longer-lived trajectories and those remaining in the excited state (Table 7).

The stabilizing effect of the increase in the number of hydrogen bonds on the S$_1$ state is even more pronounced for OH- and COOH-functionalization when comparing TPE(OH)(COOH) and TPE(OH)$_2$(COOH)$_2$ (compare Figures S20e and S20f). In the former case, 95% (19 trajectories, one decays at ~ 400 fs) and 80% of trajectories relax within 200 fs in the ωB97XD and LC-DFTB2 simulations, respectively. Also, in this case, the OH → COOH proton transfer prevails as the driving force for the S$_1$ → S$_0$ relaxation. In particular, 100% and 50% of trajectories relax via this mechanism using the ωB97XD and LC-DFTB2 methods, respectively. On the other hand, the photodynamics of TPE(OH)$_2$(COOH)$_2$ proceeds in a significantly slower way, with only 15% and 30% relaxing to the ground state in ωB97XD and LC-DFTB2 simulations, respectively. As in the previous cases, the changes in torsional angles are largely suppressed, and the multiple hydrogen bonds do not allow for a fast relaxation due to ESPT.

ESPT is the leading relaxation mechanism also in the case of the ωB97XD dynamics of TPE(OH)(CONH$_2$) and TPE(OH)$_2$(CONH$_2$)$_2$. (Figure S20c,d) Although 40% of trajectories survive in the S$_1$ state of the latter system, the proton is transferred from OH to CONH$_2$ at the later stage of the simulations, and one can expect that the relaxation to S$_0$ will occur shortly. The same can be observed in 20% of trajectories of TPE(OH)(CONH$_2$), surviving in the S$_1$ state for 2 ps. The results of the LC-DFTB2 dynamics simulations (Figure S19c and d) correspond to those obtained with the ωB97XD method for TPE(OH)$_2$(CONH$_2$)$_2$. Similar to OH- and CHO-, COOH-functionalization, the photocyclization prevails also in the LC-DFTB2 dynamics simulations of TPE(OH)(CONH$_2$) (Table 7).

The above-described results show dramatic effects of hydrogen bonds that restrict the motion of the whole system but introduce the ESPT mechanism capable of ultra-fast relaxation.

24

The ESPT occurs in all cases via the proton transfer from the phenol ring despite a significantly stronger acidity of C_6H_5COOH than C_6H_5OH in the ground state. Comparison of the dynamics simulations for single- and double functionalization of the phenyl rings (*e.g.*, TPE(OH)(CONH$_2$) and TPE(OH)$_2$(CONH$_2$)$_2$) shows blocking of the photocyclization mechanism in the latter due to the more complex hydrogen bond formation, resulting in only one available relaxation mechanism, i.e., ESPT. The dynamics of TPE(OH)$_2$(COOH)$_2$ provides promising results, showing that the hydrogen bond chain can stabilize the excited state under the circumstances in which steric hindrances combine with the strengths of hydrogen bonds.

4 Conclusions

Two types of functionalization of TPE, using strongly electron-withdrawing CN groups and hydrogen bond-forming groups, were presented to determine their excited state properties and the possibilities to inhibit ultrafast deactivation to the ground state. The excited-state behavior of selected functionalized TPE-based compounds was studied by calculations of the optical spectra and photodynamics simulations using the ωB97XD and LC-DFTB2 methods. Good agreement between the two methods obtained from the calculations of absorption spectra and excited-state minima characterization justifies using the more approximate but computationally much more efficient DFTB method especially for photodynamics investigations for longer simulation times.

Notably, the electronic transitions in excited states include for all types of substitutions solely π-orbitals. From the group I compounds based primarily on CN substitution, the functionalization with CN groups alone does not modify the character of the excited state dynamics of TPE in TPE(CN) and TPE(CN)$_5$; it only slows down the relaxation process of the latter. The main relaxation process in these systems proceeds via simultaneous distortion of the ethylene π-bond and planarization of the phenyl rings, eventually leading to photocyclization. When additional substitutions by CF$_3$ groups are introduced (TPE(CN)$_5$(CF$_3$)), the radiationless deactivation to the ground state is completely quenched due to their bulky size keeping the molecule in the excited state for the whole duration of the simulation time. The analysis of the photodynamics of TPE(CN)$_5$(CF$_3$) with TPE(CN) and TPE(CN)$_5$ leads to the conclusion that primarily steric effects are responsible for the restriction to reach the conical intersection. The effect of replacing the CF$_3$ group by OH (TPE(CN)$_5$(OH)) is twofold: restricted torsional

movement due to the hydrogen bonds formation between the OH and CN groups is completed by an ultrafast relaxation to the ground state due to OH $\rightarrow$ CN ESPT. Frequent ESPT processes were observed in the photodynamics of TPE functionalized with the second type of functional groups, able to form extensive hydrogen bonded networks. Co-existing hydrogen bonds completely block mechanisms based on internal movements making ESPT the only available relaxation mechanism. Comparison of the photodynamics simulations of singly- and doubly-functionalized (TPE(OH)(CHO), TPE(OH)(NH$_2$), and TPE(OH)(COOH) vs. (TPE(OH)$_2$(CHO)$_2$, TPE(OH)$_2$(NH$_2$)$_2$, and TPE(OH)$_2$(COOH)$_2$) show that excited states can be stabilized with the extension of the number of hydrogen bonds and, therefore, strongly inhibit the counter-productive ultrafast deactivation to the ground state.. Thus, our calculations demonstrate that either by systematic increase of bulkier groups or by introducing rigid hydrogen bonded networks, fluorescence of TPE compounds should be achievable in solution. Comparison of the dynamics simulations obtained with ωB97XD and LC-DFTB shows a larger preference of the former method for ESPT process for the excited state relaxation. Despite this difference, the results obtained with these methods lead to encouraging conclusions concerning the reliability of the latter method, which open up wide possibilities for applications in photodynamical simulations.

Conflicts of Interest

There are no conflicts to declare

Supporting Information

Vertical excitation of all investigated compound at ωB97xD and TD-LC-DFTB2 levels, HOMO and LUMO orbitals, simulated UV spectra time, graphs describing the time evolution of selected trajectories, and Cartesian coordinates for optimized structures in the ground and first excited states.

Acknowledgments

References

1. Y. Chen, J. W. Y. Lam, R. T. K. Kwok, B. Liu and B. Z. Tang, *Materials Horizons*, 2019, **6**, 428-433.
2. H. Zhang, Z. Zhao, A. T. Turley, L. Wang, P. R. McGonigal, Y. Tu, Y. Li, Z. Wang, R. T. K. Kwok, J. W. Y. Lam and B. Z. Tang, *Adv. Mater.*, 2020, **32**, 2001457.
3. Y. Hong, J. W. Y. Lam and B. Z. Tang, *Chem. Commun.*, 2009, 4332-4353.
4. Z. Lu, S. Yang, X. Liu, Y. Qin, S. Lu, Y. Liu, R. Zhao, L. Zheng and H. Zhang, *J. Mater. Chem. C*, 2019, **7**, 4155-4163.
5. M. Kaur, H. Kaur, M. Kumar and V. Bhalla, *Chem. Rec.*, 2021, **21**, 240-256.
6. S. Huang, J. Ding, A. Bi, K. Yu and W. Zeng, *Adv. Opt. Mat.*, 2021, **2100832**, 1.
7. Z. Zhao, J. W. Y. Lam and B. Z. Tang, *J. Mater. Chem.*, 2012, **22**, 23726-23740.
8. J. Chen, C. C. W. Law, J. W. Y. Lam, Y. Dong, S. M. F. Lo, I. D. Williams, D. Zhu and B. Z. Tang, *Chem. Mater.*, 2003, **15**, 1535-1546.
9. Z. Zhao, H. Zhang, J. W. Y. Lam and B. Z. Tang, *Angew. Chem., Int. Ed.*, 2020, **59**, 9888-9907.
10. W. Z. Yuan, P. Lu, S. Chen, J. W. Y. Lam, Z. Wang, Y. Liu, H. S. Kwok, Y. Ma and B. Z. Tang, *Adv. Mater.*, 2010, **22**, 2159-2163.
11. H. Zhang, X. Zheng, N. Xie, Z. He, J. Liu, N. L. C. Leung, Y. Niu, X. Huang, K. S. Wong, R. T. K. Kwok, H. H. Y. Sung, I. D. Williams, A. Qin, J. W. Y. Lam and B. Z. Tang, *J. Am. Chem. Soc.*, 2017, **139**, 16264-16272.
12. D. D. La, S. V. Bhosale, L. A. Jones and S. V. Bhosale, *ACS Applied Materials & Interfaces*, 2018, **10**, 12189-12216.
13. T. Tran, A. Prlj, K.-H. Lin, D. Hollas and C. Corminboeuf, *Phys. Chem. Chem. Phys.*, 2019, **21**, 9026-9035.
14. Q. Li and L. Blancafort, *Chem. Commun.*, 2013, **49**, 5966-5968.
15. X.-L. Peng, S. Ruiz-Barragan, Z.-S. Li, Q.-S. Li and L. Blancafort, *J. Mater. Chem. C*, 2016, **4**, 2802-2810.
16. L. Blancafort, R. Crespo and Q. Li, *Chemistry - An Asian Journal*, 2018, **14**.
17. J. Mei, N. L. C. Leung, R. T. K. Kwok, J. W. Y. Lam and B. Z. Tang, *Chem. Rev.*, 2015, **115**, 11718-11940.
18. C. Zhu, R. T. K. Kwok, J. W. Y. Lam and B. Z. Tang, *ACS Applied Bio Materials*, 2018, **1**, 1768-1786.
19. X. He, L.-H. Xiong, Z. Zhao, Z. Wang, L. Luo, J. W. Y. Lam, R. T. K. Kwok and B. Z. Tang, *Theranostics*, 2019, **9**, 3223-3248.
20. H. Zhang, Z. Zhao, P. R. McGonigal, R. Ye, S. Liu, J. W. Y. Lam, R. T. K. Kwok, W. Z. Yuan, J. Xie, A. L. Rogach and B. Z. Tang, *Materials Today*, 2020, **32**, 275-292.
21. Y. Cai, L. Du, K. Samedov, X. Gu, F. Qi, H. H. Y. Sung, B. O. Patrick, Z. Yan, X. Jiang, H. Zhang, J. W. Y. Lam, I. D. Williams, D. Lee Phillips, A. Qin and B. Z. Tang, *Chemical Science*, 2018, **9**, 4662-4670.
22. H. Zhang, J. Liu, L. Du, C. Ma, N. L. C. Leung, Y. Niu, A. Qin, J. Sun, Q. Peng, H. H. Y. Sung, I. D. Williams, R. T. K. Kwok, J. W. Y. Lam, K. S. Wong, D. L. Phillips and B. Z. Tang, *Mater. Chem. Front.*, 2019, **3**, 1143-1150.
23. J. Guan, R. Wei, A. Prlj, J. Peng, K.-H. Lin, J. Liu, H. Han, C. Corminboeuf, D. Zhao, Z. Yu and J. Zheng, *Angew. Chem., Int. Ed.*, 2020, **59**, 14903-14909.

24.   M. P. Aldred, C. Li and M.-Q. Zhu, *Chem.Eur.J.*, 2012, **18**, 16037-16045.
25.   G. Huang, B. Ma, J. Chen, Q. Peng, G. Zhang, Q. Fan and D. Zhang, *Chem.Eur.J.*, 2012, **18**, 3886-3892.
26.   B. I. Greene, *Chem. Phys. Lett.*, 1981, **79**, 51-53.
27.   E. Lenderink, K. Duppen and D. A. Wiersma, *J. Phys. Chem.*, 1995, **99**, 8972-8977.
28.   J. Ma, G. B. Dutt, D. H. Waldeck and M. B. Zimmt, *J. Am. Chem. Soc.*, 1994, **116**, 10619-10629.
29.   K. Kokado, T. Machida, T. Iwasa, T. Taketsugu and K. Sada, *J. Phys. Chem. C*, 2018, **122**, 245-251.
30.   S. Kayal, K. Roy and S. Umapathy, *J. Chem. Phys.*, 2018, **148**, 024301.
31.   P. F. Barbara, S. D. Rand and P. M. Rentzepis, *J. Am. Chem. Soc.*, 1981, **103**, 2156-2162.
32.   N. B. Shustova, T.-C. Ong, A. F. Cozzolino, V. K. Michaelis, R. G. Griffin and M. Dincă, *J. Am. Chem. Soc.*, 2012, **134**, 15061-15070.
33.   Z. Yang, W. Qin, N. L. C. Leung, M. Arseneault, J. W. Y. Lam, G. Liang, H. H. Y. Sung, I. D. Williams and B. Z. Tang, *J. Mater. Chem. C*, 2016, **4**, 99-107.
34.   N.-W. Tseng, J. Liu, J. C. Y. Ng, J. W. Y. Lam, H. H. Y. Sung, I. D. Williams and B. Z. Tang, *Chemical Science*, 2012, **3**, 493-497.
35.   G.-J. Zhao, K.-L. Han, Y.-B. Lei and Y.-S. Dou, *J. Chem. Phys.*, 2007, **127**, 094307.
36.   Y.-J. Gao, X.-P. Chang, X.-Y. Liu, Q.-S. Li, G. Cui and W. Thiel, *J. Phys. Chem. A*, 2017, **121**, 2572-2579.
37.   A. Humeniuk and R. Mitrić, *J. Chem. Phys.*, 2015, **143**, 134120.
38.   V. Lutsker, B. Aradi and T. A. Niehaus, *J. Chem. Phys.*, 2015, **143**, 184107.
39.   J. J. Kranz, M. Elstner, B. Aradi, T. Frauenheim, V. Lutsker, A. D. Garcia and T. A. Niehaus, *J. Chem. Theory Comput.*, 2017, **13**, 1737-1747.
40.   A. Prlj, N. Došlić and C. Corminboeuf, *Phys. Chem. Chem. Phys.*, 2016, **18**, 11606-11609.
41.   N. L. C. Leung, N. Xie, W. Yuan, Y. Liu, Q. Wu, Q. Peng, Q. Miao, J. W. Y. Lam and B. Z. Tang, *Chem. Eur. J.*, 2014, **20**, 15349-15353.
42.   J. Shi, N. Chang, C. Li, J. Mei, C. Deng, X. Luo, Z. Liu, Z. Bo, Y. Q. Dong and B. Z. Tang, *Chem. Commun.*, 2012, **48**, 10675-10677.
43.   T. Zhang, G. Zhu, L. Lin, J. Fan, G. Gong, J. Mu, L.-B. Xing, Y. Xie and S. Zhuo, *Chem. Phys. Lett.*, 2019, **727**, 25-30.
44.   Y. Tu, J. Liu, H. Zhang, Q. Peng, J. W. Y. Lam and B. Z. Tang, *Angew. Chem., Int. Ed.*, 2019, **58**, 14911-14914.
45.   H. Zhang, Y. Nie, J. Miao, D. Zhang, Y. Li, G. Liu, G. Sun and X. Jiang, *J. Mater. Chem. C*, 2019, **7**, 3306-3314.
46.   G.-J. Zhao and K.-L. Han, *Acc. Chem. Res.*, 2012, **45**, 404-413.
47.   P. Zhou and K. Han, *Acc. Chem. Res.*, 2018, **51**, 1681-1690.
48.   Y. Li, F. Siddique, A. J. A. Aquino and H. Lischka, *J. Phys. Chem. A*, 2021, **125**, 5765-5778.
49.   J.-D. Chai and M. Head-Gordon, *Phys. Chem. Chem. Phys.*, 2008, **10**, 6615-6620.
50.   A. Schäfer, H. Horn and R. Ahlrichs, *J. Chem. Phys.*, 1992, **97**, 2571-2577.
51.   A. Schäfer, C. Huber and R. Ahlrichs, *J. Chem. Phys.*, 1994, **100**, 5829-5835.
52.   V. Q. Vuong, J. Akkarapattiakal Kuriappan, M. Kubillus, J. J. Kranz, T. Mast, T. A. Niehaus, S. Irle and M. Elstner, *J. Chem. Theory Comput.*, 2018, **14**, 115-125.
53.   M. Elstner, D. Porezag, G. Jungnickel, J. Elsner, M. Haugk, T. Frauenheim, S. Suhai and G. Seifert, *Phys. Rev. B*, 1998, **58**, 7260-7268.

54. M. Gaus, Q. Cui and M. Elstner, *J. Chem. Theory Comput.*, 2011.

55. T. Kubař, Z. Bodrog, M. Gaus, C. Köhler and M. Elstner, *J. Chem. Theory Comput.*, 2013, **9**, 2939-2949.

56. T. A. Niehaus, M. Elstner, T. Frauenheim and S. Suhai, *J. Mol. Struct.: Theochem*, 2001, **541**, 185-194.

57. L. Zhechkov, T. Heine, S. Patchkovskii, G. Seifert and H. A. Duarte, *J. Chem. Theory Comput.*, 2005.

58. A. K. Rappe, C. J. Casewit, K. S. Colwell, W. A. I. Goddard and W. M. J. Skiff, *J. Am. Chem. Soc.*, 1992, **114**, 10024-10035.

59. R. Crespo-Otero and M. Barbatti, *Theor. Chem. Acc.*, 2012, **131**, 1-14.

60. M. Barbatti, A. J. A. Aquino and H. Lischka, *Phys. Chem. Chem. Phys.*, 2010, **12**.

61. E. Wigner, *Phys. Rev.*, 1932, **40**, 749-759.

62. J. C. Tully, *J. Chem. Phys.*, 1990, **93**, 1061-1071.

63. G. Granucci and M. Persico, *J. Chem. Phys.*, 2007, **126**, 134114.

64. S. Hammes‑Schiffer and J. C. Tully, *J. Chem. Phys.*, 1994, **101**, 4657-4667.

65. G. Granucci, M. Persico and A. Toniolo, *J. Chem. Phys.*, 2001, **114**, 10608-10615.

66. F. Plasser and H. Lischka, *Journal of Chemical Theory & Computation*, 2012, **8**, 2777-2789.

67. F. Plasser, R. Crespo-Otero, M. Pederzoli, J. Pittner, H. Lischka and M. Barbatti, *J. Chem. Theory Comput.*, 2014, **10**, 1395-1405.

68. F. Siddique, M. Barbatti, Z. Cui, H. Lischka and A. J. A. Aquino, *J. Phys. Chem. A*, 2020, **124**, 3347-3357.

69. B. Aradi, B. Hourahine and T. Frauenheim, *J. Phys. Chem. A* 2007, **111**, 5678-5684.

70. M. J. T. Frisch, G. W.; Schlegel, H. B.; Scuseria, G. E.; Robb, M. A.; Cheeseman, J. R.; Scalmani, G.; Barone, V.; Mennucci, B.; Petersson, G. A.; Nakatsuji, H.; Caricato, M.; Li, X.; Hratchian, H. P.; Izmaylov, A. F.; Bloino, J.; Zheng, G.; Sonnenberg, J. L.; Hada, M.; Ehara, M.; Toyota, K.; Fukuda, R.; Hasegawa, J.; Ishida, M.; Nakajima, T.; Honda, Y.; Kitao, O.; Nakai, H.; Vreven, T.; Montgomery Jr., J. A.; Peralta, J. E.; Ogliaro, F.; Bearpark, M. J.; Heyd, J.; Brothers, E. N.; Kudin, K. N.; Staroverov, V. N.; Kobayashi, R.; Normand, J.; Raghavachari, K.; Rendell, A. P.; Burant, J. C.; Iyengar, S. S.; Tomasi, J.; Cossi, M.; Rega, N.; Millam, N. J.; Klene, M.; Knox, J. E.; Cross, J. B.; Bakken, V.; Adamo, C.; Jaramillo, J.; Gomperts, R.; Stratmann, R. E.; Yazyev, O.; Austin, A. J.; Cammi, R.; Pomelli, C.; Ochterski, J. W.; Martin, R. L.; Morokuma, K.; Zakrzewski, V. G.; Voth, G. A.; Salvador, P.; Dannenberg, J. J.; Dapprich, S.; Daniels, A. D.; Farkas, Ö.; Foresman, J. B.; Ortiz, J. V.; Cioslowski, J.; Fox, D. J. , *Gaussian 09, Gaussian, Inc.: Wallingford, CT, USA*, 2009.

71. M. Barbatti, M. Ruckenbauer, F. Plasser, J. Pittner, G. Granucci, M. Persico and H. Lischka, *WIREs Comp. Mol. Sci.*, 2014, **4**, 26-33.

72. H. Wu, Y. Jiang, Y. Ding, Y. Meng, Z. Zeng, C. Cabanetos, G. Zhou, J. Gao, J. Liu and J. Roncali, *Dyes Pigm.*, 2017, **146**, 323-330.

73. B. H. Brandsen, *Physics of Atoms and Molecules*, Longman Group Limited: London, New York 1983.